Scientific Research Publishing

World Journal of Condensed Matter Physics, 2024, 14, 51-65
https://www.scirp.org/journal/wjcmp
ISSN Online: 2160-6927
ISSN Print: 2160-6919

Monte Carlo Simulations of Doping Properties of a Spin-3/2 Ising Nanotube

Sènan Ida Valérie Hontinfinde[1*], Noèl Odjo[1,2], Joèl Kple[2,3], Ansèlme Kpadonou[4], Félix Hontinfinde[2,3]

[1]Ecole Nationale Supérieure de Génie Mathématique et Modélisation (ENSGMM), UNSTIM, Abomey, Benin
[2]Faculté des Sciences et Techniques, Université d'Abomey-Calavi, Abomey-Calavi, Benin
[3]Institut de Mathématique et de Sciences Physiques, Université d'Abomey-Calavi, Abomey-Calavi, Benin
[4]Ecole Normale Supérieure, UNSTIM, Natitingou, Benin
Email: *vhontinfinde26@gmail.com

How to cite this paper: Hontinfinde, S.I.V., Odjo, N., Kple, J., Kpadonou, A. and Hontinfinde, F. (2024) Monte Carlo Simulations of Doping Properties of a Spin-3/2 Ising Nanotube. *World Journal of Condensed Matter Physics*, **14**, 51-65.
https://doi.org/10.4236/wjcmp.2024.143006

Received: May 3, 2024
Accepted: July 5, 2024
Published: July 8, 2024

Abstract

The effect of spin-1 impurities doping on the magnetic properties of a spin-3/2 Ising nanotube is investigated using Monte Carlo simulations within the Blume-Emery-Griffiths model in the presence of an external magnetic field. The thermal behaviors of the order parameters and different macroscopic instabilities as well as the hysteretic behavior of the material are examined in great detail as a function of the dopant density. It is found that the impurities concentration affects all the system magnetic properties generating for some specific values, compensation points and multi-cycle hysteresis. Doping conditions where the saturation/remanent magnetization and coercive field of the investigated material can be modified for permanent or soft magnets synthesis purpose are discussed.

Keywords

Doped Ising Nanotube, Monte Carlo Simulations, Compensation Point, Phase Transitions, Coercive Field

1. Introduction

In recent decades, an intense effort has been devoted to the synthesis of various nanostructured materials [1]-[9]. In particular, doping of single materials with impurities to achieve rich multifunctionality by deft combination of different physical properties has been a topic of considerable interest due to potential applications as nanowires, data storage, spin valves, quantum electromagnets, nanoelectronic and spintronic devices (see [10] [11] and references therein). This

leads to the generation of new energy levels in the material's band gap with the associated electronic states and constitutes a key step in the synthesis of electronic and magnetic devices [10] [11]. In particular, the incorporation of magnetic atoms in nanoparticles (NPs) could result in materials with novel magneto-transport properties requested in spintronics and magnetomagnets. In that case, it is crucial to know which elements can be appropriate with best bonds to the NPs and how the magnetic properties are affected by the presence of such elements. Some interesting results have been recently achieved in Refs. [11]-[13] in the enhancement of magnetic characteristics of various NPs through doping procedure. For nitrogen incorporation into carbon nanotubes (N-CNT) for example, various approaches have been used including magnetron sputtering technique, arc-discharge in nitrogen atmosphere, etc. [14] [15]. The N-CNT has been also synthesized by a hydrothermal adsorption method in Ref. [16]. While doping of bulk materials can be easily achieved, that of nanostructured semiconductors has proven difficult. An efficient and facile synthesized method of titanium-dioxide (TiO_2) nanotubes has been however reported in Ref. [17]. Usually, the effect of dopants on materials' optical, electronic and magnetic properties are theoretically addressed by means of first principes density functional theory (DFT) calculations and numerous works exist in the literature in the field [10] [18] [19].

In material doping, the resulting bands do not depend only on impurities concentration but also on various other parameters, in particular the way dopants are distributed in the unit cell under consideration. Thus, in a theoretical investigation of materials doping, one should take into consideration these aspects to generate reliable predictions. A random distribution of the impurities may be used with an average of physical quantities over such distribution (see discussions in Ref. [20]). This procedure is however computationally very expensive. Fast diffusion Monte Carlo sampling via conformal map [21] may be an efficient calculation method. As a consequence, doping studies using simulations of nanomagnets described by classical spins hamiltonians are lacking in the literature. This fact motivates the present study where an Ising nanotube constituted by atoms of spins 3/2 is doped by substitution of atoms of spins 1. Magnetic nanotubes modelling using Ising systems has been considered in several recent works. Several approaches have been used, particularly statistical-mechanical methods including the Mean-Field (MF) theory [22], the Effective Field Theory (EFT) [23] [24], numerical simulations by Monte Carlo (MC) [25]-[27] or Cellular Automata (CA) [28], etc. Some attracting magnetic properties have been reported on Ising nanotubes in references [29]-[31].

Researchers have found several ways to improve the saturation/remanent magnetization and coercivity by materials doping. Indeed, Bhushan *et al.* [11] studied Ba and Ca co-doping of $BiFeO_3$ and searched for conditions in which simultaneous enhancement of coercive field and saturation magnetization could occur. Also, Apostolova *et al.* [12] using a modified Heisenberg model studied the effect of ion-doping on magnetic, optical and phonon properties of MgO

NPs. They found that this doping could enhance the coercive field. Manglam *et al.* also studied the enhancement of coercivity as well as saturation magnetization of M-type Barium Hexaferrite (BHF) by Ho-doping [13]. In the present work, the spin-3/2 nanotube under consideration is described by means of the microscopic Blume, Emery and Griffiths (BEG) model [32]. After calculating magnetic properties of the original nanotube, in particular the behaviors of order parameters and phase transitions with physical parameters, atoms of spins 3/2 are progressively replaced by atoms of spins 1 with a well-determined density or concentration and the resulting magnetic properties are calculated. We are mostly interested in the behaviors of the critical temperature, the remanent magnetization (M_r) and the coercive field (H_c) that can be evaluated through the hysteretic behavior of the doped materials. We found through our calculations beyond usual properties as critical and compensation temperatures, that for suitable values of the dopant density, it is possible to modulate the coercive field in view to synthesize soft or permanent magnets for various applications.

The paper is organized as follows. In Section 2, the model is formulated. Section 3 gives briefly the MC simulations method. In Section 4, numerical results and discussion are provided. Section 5 is devoted to concluding remarks.

2. Model and Formalism

A two-hexagonal layer nanotube model is considered. The nanotube consists of $N_z = 300$ sections in the z-direction where periodic boundary conditions are assumed. Some few results have been provided on a less longer system comprising only 10 sections. Each section laying in the *xy*-plane (**Figure 1**) contains 30 atoms. The sections stacking procedure used has been adopted in several previous works [27] [33]. Each section spin is connected to the two nearest-neighbor spins on the above and below sections. The interaction hamiltonian is defined as follows [32]:

$$\begin{aligned} H = & -J_1 \sum_{\langle ij \rangle} \sigma_i \sigma_j - J_1 \sum_{\langle kl \rangle} S_k S_l - J_2 \sum_{\langle ik \rangle} \sigma_i S_k - K \sum_{\langle ij \rangle} \sigma_i^2 \sigma_j^2 - K \sum_{\langle kl \rangle} S_k^2 S_l^2 \\ & - K \sum_{\langle ik \rangle} \sigma_i^2 S_k^2 - \Delta \sum_i (\sigma_i)^2 - \Delta \sum_k (S_k)^2 - h \left(\sum_i \sigma_i + \sum_k S_k \right) \end{aligned} \quad (1)$$

where the summation indices $\langle ij \rangle$, $\langle jk \rangle$ and $\langle kl \rangle$ denote a summation over all pairs of neighboring spins. J_1/J_2 is the exchange coupling constant between two nearest-neighbor spins of the same/different types, K is the quadrupolar interaction and Δ is the lattice anisotropy constants. We consider only the case of an uniaxial anisotropy (z) axis the same for all ions. The parameter h is an uniform external magnetic field applied parallel to the anisotropy (z) axis. The field acts on all spins $S_i = S_i^z$ and $\sigma_i = \sigma_i^z$ [27]. In the numerical simulations of the model, only the case $J_1 = -J_2 = 1$ is considered. It is worth noting that in the original nanotube, there is no site k of spin S_k.

3. Monte Carlo Simulation

The standard Metropolis algorithm is adopted [33]-[35]. The approach

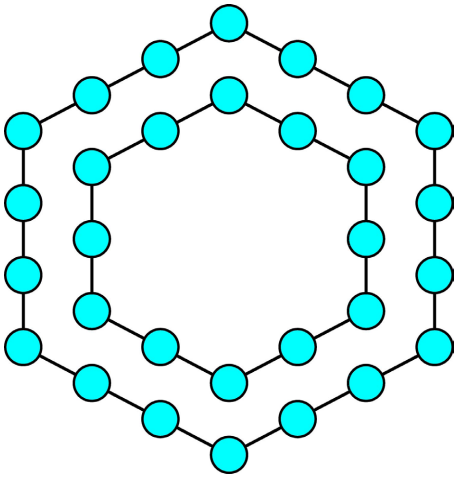

Figure 1. (Colour online) Schematic representation of a section of a two-hexagonal nanotube constituted of atoms of spins 3/2 in the *xy*-plane. In the z-direction, sections are stacked in a way that a section atom has one neighboring atom in the below section and one above. The last section and the first one are neighboring sections due to periodic boundary conditions assumed in the z-direction.

involves several sequential steps. An impurities density is first selected. For a giving distribution of the dopant in the nanotube, an atom is randomly selected. Then, one chooses randomly one of its spin value within the possible projections with an uniform distribution probability. Another random number is chosen to decide or reject the attempted move. Physical quantities are evaluated after $n_s = 10^5$ to $n_s = 2\times10^5$ MC steps per site are performed. The first $n_e = 25\times10^3$ steps are taken for thermal equilibration and discarded in the averaging procedure. Two to five independent runs are often performed to get smooth data. The results are then averaged over at least 50 distributions of the dopant in the nanotube for a given dopant concentration. Since periodic boundary conditions are set on the system, we believe that this number can help in getting some insight into the doping magnetic properties of the nanotube. Denoting by N, the number of atoms in the nanotube, average values of the magnetizations are evaluated as follows:

$$M = \frac{1}{N}\left(\sum_i \sigma_i + \sum_k S_k\right) \tag{2}$$

At the critical temperature T_c of the system, M vanishes continuously and the magnetic susceptibility χ should diverge. This quantiy has the expression:

$$\chi = \frac{1}{k_B T}\left(\left\langle M^2\right\rangle - \left\langle M\right\rangle^2\right) \tag{3}$$

where k_B is the Boltzmann constant, and $\langle . \rangle$ denotes a statistical average over the number of MC steps needed to reach the steady state, starting from thermal equilibrium. A peak in the behavior of χ often indicates a macroscopic instability in a finite system.

4. Results and Discussion

In the results, coupling constants J_1, J_2 and K, crystal-field Δ, magnetic field h and the temperature T are expressed in units of a certain energy J.

4.1. Magnetic Properties of the Nanotube

We first performed a finite-size analysis of the system in view to give some insight into the nanotube diameter D effect on the magnetic properties, in particular on T_c for selected values of the crystal-field Δ. For that, three different nanotube diameters D are investigated with the following total number of magnetic atoms in each section: $N_s = 18; 30; 42$. As it can be observed from **Figure 2**, all nanotube magnetizations decrease and vanish continuously. The following transition temperatures T_c associated to the maximum of the magnetic susceptibility χ related to each nanotube diameter are got: $T_c\left(N_s = 18\right) = 4.4; 5.2; 5.6$, $T_c\left(N_s = 30\right) = 4.6; 5.3; 5.8$, $T_c\left(N_s = 42\right) = 4.7; 5.4; 5.9$ for $\Delta = -1; 0; +1$ respectively. These results revealed several properties. They first indicated that T_c increases with increasing values of D and Δ. Second, they showed that the observed transitions are of second order. Indeed, for first-order transitions, the maximum of χ should scale with the total number of magnetic atoms in the system as: $\chi_{\max} \simeq D^b$ where b is the scaling exponent related to the system dimensionality or simply $\chi_{\max} \simeq N$ [36]. This is truly not the case in **Figure 2** for values of Δ selected. For these calculations, the quadrupolar parameter K is set to zero. In the following, K is fully taken into consideration and the system of size $N_s = 30$ is selected. This allows one to draw some phase diagrams in the (T_c, Δ) plane for varying values of K and in the (T_c, K) plane for varying values of Δ. The achieved results are illustrated in **Figure 3(a)** and **Figure 3(b)**. In **Figure 3(a)**, it emerges that for large and negative values of Δ, the transition lines are parallel to the Δ-axis with almost no influence of the parameter K. These results are consistent with those reported in **Figure 4** of Ref. [33]. For Δ greater than -4, T_c decreases with increasing values of K. For fixed values of K and varying Δ, T_c increases, passes through a maximum and then decreases. Values of Δ associated to the maximum of T_c-lines decrease with increasing values of K and T_c-lines almost show a parabolic form. These results are consistent with those found in Refs. [27] [33]. Above T_c-lines, the system lays in the paramagnetic phase with zero average magnetization M. Below, ferromagnetic phases are got. In **Figure 3(b)**, T_c-lines show completely different trends except at large and negative values of Δ. For specific values of Δ, a monotonic decrease of $T_c(K)$ is observed while for others, a maximum is seen in the behavior of the phase boundaries. Values of K associated to this maximum, shift to the right with increasing absolute values of Δ.

The system revealed some interesting hysteretic properties within the physical parameters space in the presence of an external field. Properties are calculated with $n_s = 10^3$ MC steps per site and $n_e = 100$ MC steps for thermal equilibration of the initial configuration. **Figure 4** illustrates the behavior of the remanent

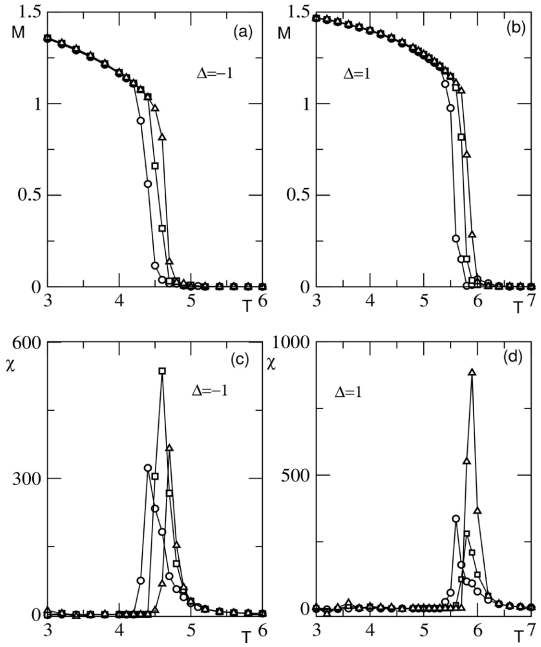

Figure 2. Nanotube magnetizations M (a, b) and associated response functions χ (c, d) as a function of the temperature T for three nanotube section sizes: $N_s = 18$ (circles), $N_s = 30$ (squares) and $N_s = 42$ (triangles) and $\Delta = -1; 1$. The maximum of χ is associated to the transition temperature T_c. It results that T_c increases with the nanotube diameter D. The parameter K is set to zero in the calculations.

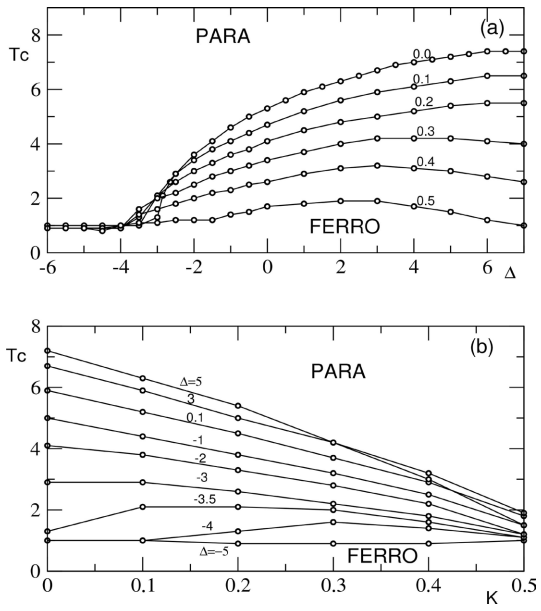

Figure 3. Phase boundaries of the spin-3/2 nanotube in the (T_c, Δ) plane (panel a) for selected values of K and in the (T_c, K) plane (panel b) for values of Δ specified in the panel. For large and negative values of Δ (panels a and b), T_c is almost constant in the range of K investigated. It could be remarked that non-zero values of K manages to bend the transition lines to the Δ-axis in panel a. Values of Δ associated to the maximum of T_c-lines decrease with increasing K.

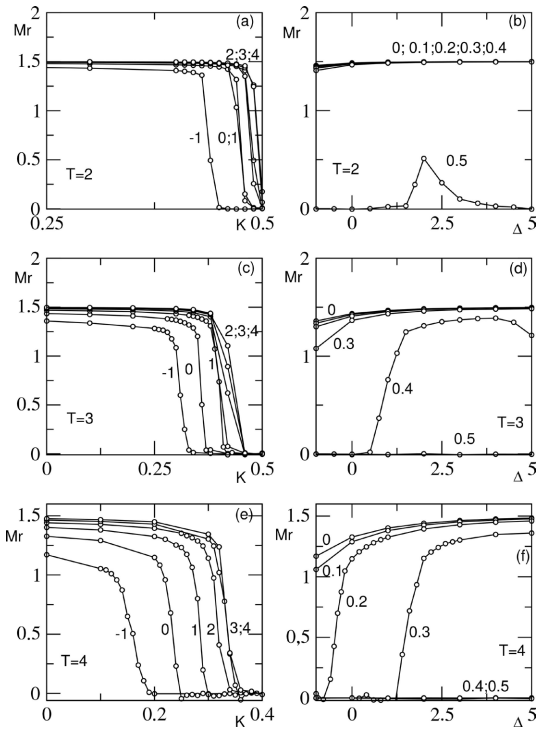

Figure 4. Remanent magnetization M_r as a function of the parameter K at selected values of Δ (panels a, c, e). In panels b, d, f, M_r is illustrated as function of Δ for selected values of K written on the curves. Calculations are performed at three temperatures: $T = 2; 3; 4$. An increase of T, Δ or K has a reducing effect on M_r.

magnetization M_r at selected values of T and varying values of K and Δ. One sees that large values of K lead to $M_r = 0$ which may be associated to a critical hysteresis and an ideal soft magnet. For sufficiently low values of K, the system shows a M_r of high amplitude. From the figure, it also emerges that an increase of Δ reduces the disordering influence of K. At very low temperature, large domains of K and Δ in which M_r keeps an important value exist. This observation may indicate that rock permanent magnets may be observed in cold regions for materials with large and positive values of Δ and small values of K. We also studied the behavior of M_r as a function of Δ for some selected values of parameters K and T. It results that at low T, the parameters K and Δ have almost no effect on M_r as far as K remains small. As T is raised, M_r becomes quite small at relatively large values of K and small values of Δ. The coercive field H_c has been also estimated for selected values of K and T and varying values of Δ (**Figure 5**). H_c increases with Δ, then either passes by a maximum or saturates with some fluctuations at large values of Δ. At all selected temperatures, H_c is maximal for $K = 0$. Thus very low values of K is required to get high coercive field for the system.

4.2. Doping Effects on Nanotube Properties

In the case of nanotube doping by atoms of spins 1, we distinguished as already

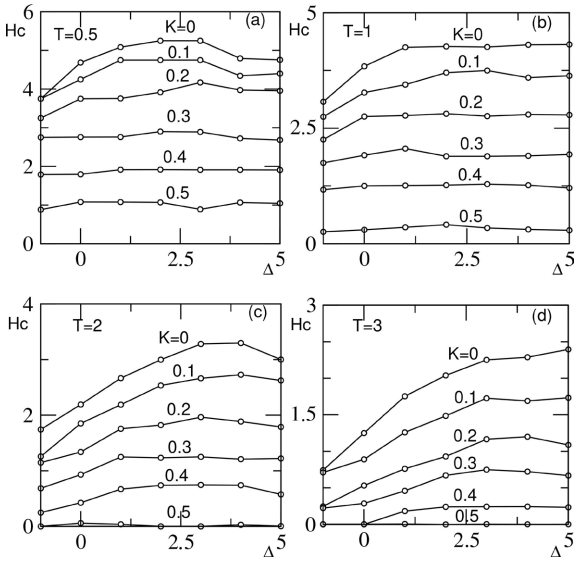

Figure 5. Coercive field H_c as a function of Δ for selected values of K and T specified in different panels. H_c is almost constant at low values of T and large values of K. At high T, it increases with Δ and shows a maximum which value decays with increasing values of K.

stated above, two nearest-neighbor interactions. Indeed, between atoms of the same nature, the interaction is ferromagnetic and antiferromagnetic otherwise. Denoting by c the impurities concentration, $9000c$ atoms of spins 3/2 with varying c, are replaced by atoms of spins 1. We performed an average of physical quantities over $n=50$ random configurations of these atoms in the nanotube. Theoretically, the appropriate number n is very large and numerical calculations are computationally too costly. This number is of course reduced due to periodic boundary conditions on the nanotube in the z-direction and atomic configurations invariance through symmetry operations. We believe that $n=50$ should help in getting some insight on impurities effect on physical quantities investigated in the previous subsection. We also checked that qualitative behaviors of M and T_c remain unchanged with $n=50;75;100$ for $\Delta=0;K=0$ and $\Delta=2;K=0.2$. For $\Delta=0$ and $K=0$, **Figure 6(a)**, **Figure 6(c)** illustrate results on the nanotube magnetization as a function of T for selected values of the dopant density c. It could be observed that at high T, the system lays in a disordered phase with $M=0$. At low T, a spontaneous magnetization exists. With increasing T, the magnetization M shows a continuous decrease and a critical temperature T_c above which it lays in a paramagnetic phase. It is noteworthy that with increasing parameter c, M decreases, passes through a minimum and then increases to saturate at $M=1$ which is, indeed, the magnetization of a nanotube of spins 1, all spin 3/2 atoms being replaced. It appears that for values of c of about 0.7, compensation temperatures T_{comp} were detected. T_{comp} corresponds to the temperature at which M vanishes below T_c. The existence of T_{comp} is of technological utility. Indeed, at that point magnetic immunity is achieved and the system does not respond to any external magnetic field. The advent of T_{comp}

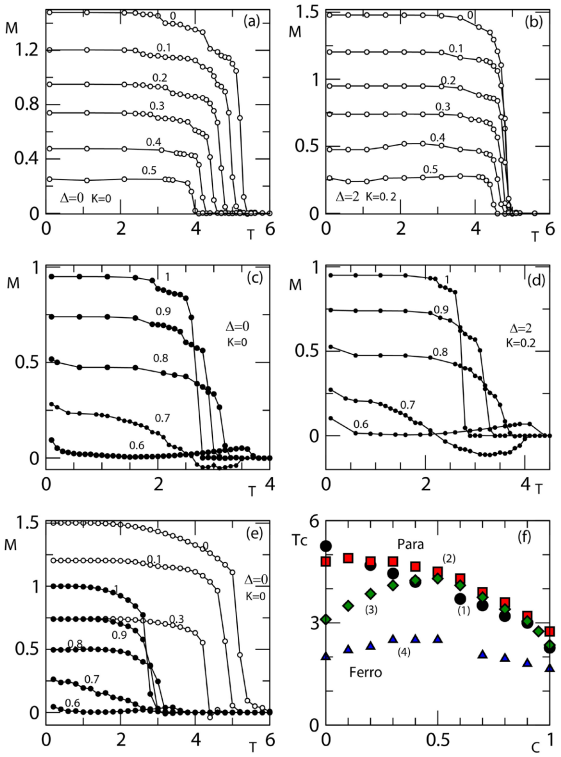

Figure 6. (Colour online) Thermal behaviors of the doped nanotube magnetization M for various values of the imputities (atoms of spin 1) density c for $\Delta = 0; K = 0$ (panels (a) and (c)) and $\Delta = 2; K = 0.2$ (panels (b) and (d)) for the system of **Figure 1**. In panel (e), results concern a system of longitudinal length $N_z = 10$ and same qualitative behaviors observed in panels (a) and (c) are recovered. In panel (f), phase diagrams are illustrated in the (T_c, c) plane for (1) $\Delta = 0$, $K = 0$; (2) $\Delta = 2$, $K = 0.2$; (3) $\Delta = 2$, $K = 0.4$; (4) $\Delta = -2$, $K = 0.4$ for the original system with $N_z = 300$. It could be observed that for c about 0.7, the model exhibits a compensation temperature T_{comp} where the magnetization vanishes before the critical temperature T_c.

is not surprising since for values about $c = 0.6$, a mixed Ising spins system which often shows compensation points is got. Indeed, for $c = 0.6$, the total magnetization of atoms of spins 1, *i.e.* $0.6 \times 1 \times N$ is almost equal to that of other atoms, $0.4 \times 3/2 \times N$. Therefore, it is likely that at a certain temperature, compensation point should occur. It could be observed that for $c = 0.6$, a wide region where M lays very close to zero is found. More calculations are needed to check whether it contains a compensation point or a paramagnetic phase embedded into two separate ferromagnetic phases. **Figure 6(e)** illustrates M calculated for a smaller system with only $N_z = 10$ and $n = 200$. The qualitative behaviors observed for M, T_c and T_{comp} in **Figure 6(a)**, **Figure 6(c)** are recovered. In **Figure 6(b)**, **Figure 6(d)**, previous calculations are reproduced for $\Delta = 2$ and $K = 0.2$. Magnetization curves show same general trends as previously observed. T_c's and T_{comp}'s are evidently different. For some c's, the temperature T_c appears higher and for others lower. In **Figure 6(f)**, some phase boundaries are

illustrated for $N_z = 300$ in the (T_c, c) plane. For $\Delta = 0$ and $K = 0$, the T_c-line is almost linear (full circles) and this trend could already be guessed from Figure 6(a), Figure 6(c). For other values, phase boundaries are nearly parabolic for relatively low values of c. Above T_c-lines, the system lays in the paramagnetic phase. Although, the situation around $c = 0.6$ needs much more investigation, it emerges through different panels of Figure 6, that parameters K, c, and Δ have a strong influence on magnetic properties of the doped nanotube. Their variation generates fundamental changes in the illustrated qualitative phase boundaries.

Figure 7 illustrates the hysteretic behavior of the system at $T = 0.5; 2.0$, $K = 0.2$ for some selected values of c. It could be observed that at $T = 0.5$, M_r increases with increasing Δ's and becomes important in magnitude at $\Delta = 1$ for relatively small value of c (panel a). The coercive field H_c shows an increase for increasing Δ in the same panel. Let us remark that for $\Delta = -5$, M shows some horizontal steps which wideness shrinks with the increase of c. The existence of these steps shows that the phase in which the system lays in this region is stabilized by the magnetic field h. It could be observed through different panels that H_c or M_r can be enhanced by acting on parameters c, Δ or K. Critical hysteresis are generated for some specific values of model parameters. An increase of T strongly affects H_c and M_r. Through Figure 7(a), Figure 7(c), Figure 7(e), for $\Delta = 1$, M_r decreases, passes by some minimum and increases again when c increases. Same observations are got for $\Delta = -3$. At crystal-field value $\Delta = -5$, critical hysteresis is got at $c = 0.6$ whereas at $c = 0.8$, the hysteresis cycle splits into two loops with $H_c = 0$ and $M_r = 0$ (not commonly observed). At $c = 0.8$ and $\Delta = 1$, three hysteresis cycles are got. The latters are required in technology for multi-memory devices. These results indicate that the material doping leads to some interesting magnetical properties required in many technological applications. It affects M_r and H_c and for suitable values of impurities concentration, multi-cycle or critical hysteresis are generated. In Figure 7(b), Figure 7(d), Figure 7(f), the temperature T is raised and more thermal spin fluctuations took place. One can observe that for $\Delta = -3; -5$, only critical hysteresis are got. These properties are more clarified when the hysteretic behaviors are investigated in the (M_r, c) plane with varying other physical parameters. Indeed in Figure 8, results on M_r for $\Delta = -4$ and $\Delta = -5$ and selected values of K showed that M_r (and evidently H_c) vanishes at about $c = 0.5$. This means that associated hysteresis should be critical for c larger than 0.5 whatever K's. Calculated H_c's for these Δ's are very small even at low values of c. For values below $c = 0.5$, hysteresis behavior exists with very minor effect of the parameter K on M_r. For $\Delta = -3$, the situation looks completely different. Indeed, a further increase is observed for M_r up to $c = 1$. For $\Delta = -2$ and beyond, K has almost no effect on the hysteretic behavior at any value of c. The behavior of H_c is quite different (Figure 9). Indeed one observes from different panels that H_c does not have a monotonic behavior. Curves H_c show a minimum at about $c = 0.6$ independently of the value of K. The latter, contrarily to observations from Figure 8,

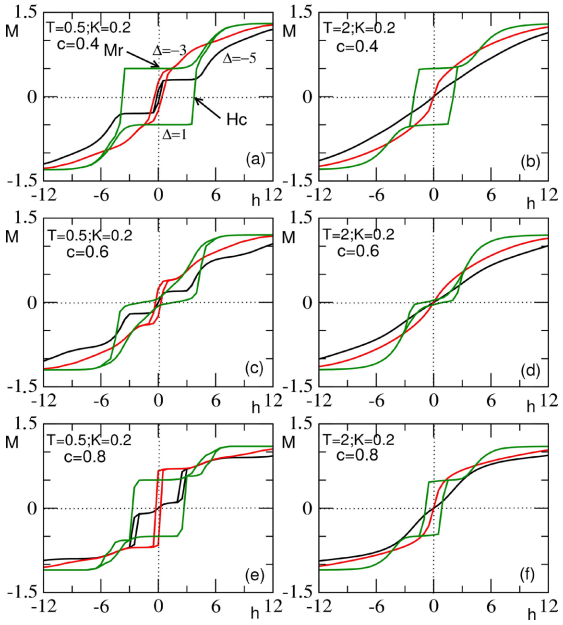

Figure 7. (Colour online) Magnetic hysteresis cycles of the doped spin-3/2 Ising nanotube. Values of physical parameters used are written in different panels. It obviously appears that the impurities density c has an important effect on the doped nanotube magnetic properties.

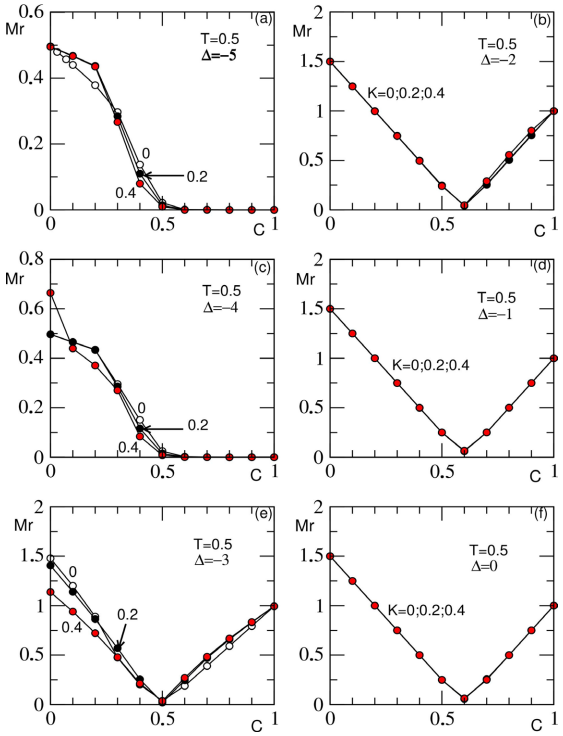

Figure 8. (Colour online) Remanent magnetization M_r as a function of the impurities density c at some selected values of model parameters. For some values of these parameters, $M_r = 0$ and the product cannot be used for a memory device. M_r is important at small and large values of c. The value of c associated to the minimum of M_r when it exists, depends on the Δ-range considered.

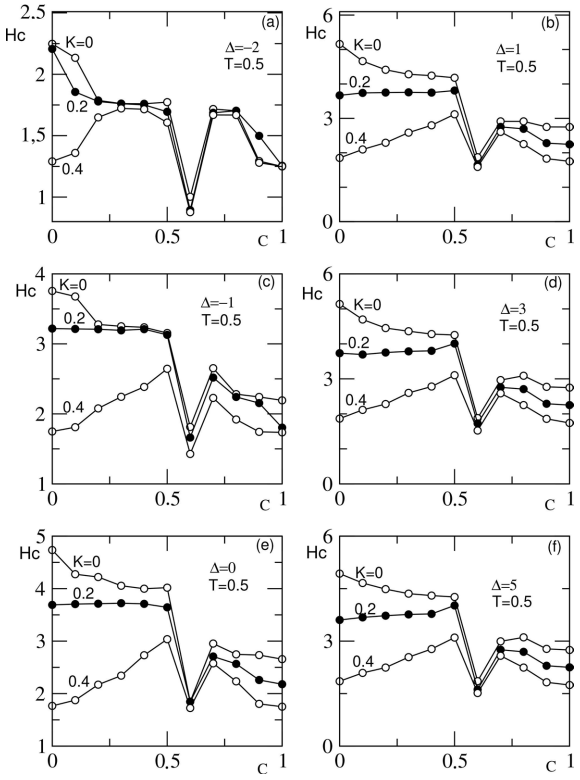

Figure 9. Coercive field H_c of the doped nanotube as a function of the impurities density c at some selected values of model parameters. It could be observed that for some specific values of the model parameters it is possible to enhance the coercive field by doping the material. This is an important issue since it can help expermenters to fabricate permanent magnets with high values of H_c and M_r.

has a strong influence on H_c at selected values of Δ. At fixed value of c, H_c is a decreasing function of K. Similar trends are observed for impurities density c larger than 0.6. It is worth noting that for $K = 0.2$ and beyond, it is possible to enhance the coercive field H_c of the nanotube to make permanent magnets for technological utilities using suitable values of c (of course below 0.5) and Δ. The observed enhancement of H_c for $K = 0.4$ and probably for larger values upon increase of dopant concentration is similar to the one obtained in **Figure 5** of Ref. [12] during doping of MgO NPs.

5. Conclusion

In this work, we studied the effect of substitution of atoms of a spin-3/2 nanotube by atoms of spins 1 on the magnetic properties of the nanotube. We used the BEG Hamiltonian and Monte Carlo simulations with Metropolis algorithm. We first studied the behavior of the critical temperature T_c of the spin-3/2 nanotube with its diameter D. We found that T_c increases with the nanotube diameter D. We also remarked that it can increase or decrease depending on values of the quadrupolar parameter strength K and the crystal-field strength Δ. Then we investigated as functions of the dopant density, critical properties and

hysteretic behaviors of the system. We observed that the dopant concentration influenced most achieved previous results, in particular the critical temperature as well as the remanent magnetization and the coercive field. We found that for suitable values of the dopant density, it is possible to alter or enhance the coercive field as well as the remanent magnetization. This is a formidable issue in the sense that this finding can help experimenters to tailor nanomaterials in view to get soft or permanent magnets since e.g. permanent magnets need moderate remanent magnetization and large coercive field [13]. It is worth noting that the system doping can generate multi-cycle hysteresis which are needed for multi-memory devices. It can also induce compensation points. The latter have crucial applications since there, the system gets a magnetic immunity and does not react with any external magnetic fields.

Author Contributions

All authors equally contribute to the present work in the calculations and in the manuscript writing process.

Conflicts of Interest

The authors declare that they have no known competing financial interests or personal relationships that could have appeared to influence the work reported in this paper.

References

[1] Skomski, R. (2003) Nanomagnetics. *Journal of Physics*: *Condensed Matter*, **15**, R841-R896. https://doi.org/10.1088/0953-8984/15/20/202

[2] Zou, Y., Klich, I. and Refael, G. (2008) Effect of Inhomogeneous Coupling on BCS Superconductors. *Physical Review B*, **77**, Article ID: 144523. https://doi.org/10.1103/physrevb.77.144523

[3] Kim, J., Park, S., Lee, J.E., Jin, S.M., Lee, J.H., Lee, I.S., *et al.* (2006) Designed Fabrication of Multifunctional Magnetic Gold Nanoshells and Their Application to Magnetic Resonance Imaging and Photothermal Therapy. *Angewandte Chemie International Edition*, **45**, 7754-7758. https://doi.org/10.1002/anie.200602471

[4] López-Ortega, A., Estrader, M., Salazar-Alvarez, G., Roca, A.G. and Nogués, J. (2015) Applications of Exchange Coupled Bi-Magnetic Hard/Soft and Soft/Hard Magnetic Core/Shell Nanoparticles. *Physics Reports*, **553**, 1-32. https://doi.org/10.1016/j.physrep.2014.09.007

[5] Kodama, R.H., Berkowitz, A.E., McNiff Jr., E.J. and Foner, S. (1996) Surface Spin Disorder in $NiFe_2O_4$ Nanoparticles. *Physical Review Letters*, **77**, 394-397. https://doi.org/10.1103/physrevlett.77.394

[6] Hayashi, T., Hirono, S., Tomita, M. and Umemura, S. (1996) Magnetic Thin Films of Cobalt Nanocrystals Encapsulated in Graphite-Like Carbon. *Nature*, **381**, 772-774. https://doi.org/10.1038/381772a0

[7] Wegrowe, J.E., Kelly, D., Jaccard, Y., Guittienne, P. and Ansermet, J.P. (1999) Current-Induced Magnetization Reversal in Magnetic Nanowires. *Europhysics Letters* (*EPL*), **45**, 626-632. https://doi.org/10.1209/epl/i1999-00213-1

[8] Fert, A. and Piraux, L. (1999) Magnetic Nanowires. *Journal of Magnetism and*

Magnetic Materials, **200**, 338-358. https://doi.org/10.1016/s0304-8853(99)00375-3

[9] McGary, P.D., Tan, L., Zou, J., Stadler, B.J.H., Downey, P.R. and Flatau, A.B. (2006) Magnetic Nanowires for Acoustic Sensors (Invited). *Journal of Applied Physics*, **99**, Article ID: 08B310. https://doi.org/10.1063/1.2167332

[10] Mananghaya, M.R. (2012) Carbon Nanotubes Doped with Nitrogen, Pyridine-Like Nitrogen Defects, and Transition Metal Atoms. *Journal of the Korean Chemical Society*, **56**, 34-46. https://doi.org/10.5012/jkcs.2012.56.1.034

[11] Bhushan, B., Das, D., Priyam, A., Vasanthacharya, N.Y. and Kumar, S. (2012) Enhancing the Magnetic Characteristics of $BiFeO_3$ Nanoparticles by Ca, Ba Co-Doping. *Materials Chemistry and Physics*, **135**, 144-149. https://doi.org/10.1016/j.matchemphys.2012.04.037

[12] Apostolova, I., Apostolov, A. and Wesselinowa, J. (2023) Magnetic, Optical and Phonon Properties of Ion-Doped MgO Nanoparticles. Application for Magnetic Hyperthermia. *Materials*, **16**, Article 2353. https://doi.org/10.3390/ma16062353

[13] Manglam, M.K., Shukla, A., Mallick, J., Yadav, M.K., Kumari, S., Zope, M., *et al.* (2022) Enhancement of Coercivity of M-Type Barium Hexaferrite by Ho Doping. *Materials Today: Proceedings*, **59**, 149-152. https://doi.org/10.1016/j.matpr.2021.10.365

[14] Suenaga, K., Johansson, M.P., Hellgren, N., Broitman, E., Wallenberg, L.R., Colliex, C., *et al.* (1999) Carbon Nitride Nanotubulite—Densely-Packed and Well-Aligned Tubular Nanostructures. *Chemical Physics Letters*, **300**, 695-700. https://doi.org/10.1016/s0009-2614(98)01425-0

[15] Droppa Jr., R., Ribeiro, C.T.M., Zanatta, A.R., dos Santos, M.C. and Alvarez, F. (2004) Comprehensive Spectroscopic Study of Nitrogenated Carbon Nanotubes. *Physical Review B*, **69**, Article ID: 045405. https://doi.org/10.1103/PhysRevB.69.045405

[16] Zhang, X., Cui, C., Zheng, Q., Wang, Y., Chang, J. and Wang, S. (2021) Development of Highly Efficient and Reusable Magnetic Nitrogen-Doped Carbon Nanotubes for Chlorophenol Removal. *Environmental Science and Pollution Research*, **28**, 37424-37434. https://doi.org/10.1007/s11356-021-13302-0

[17] Alivov, Y., Singh, V., Ding, Y., Cerkovnik, L.J. and Nagpal, P. (2014) Doping of Wide-Bandgap Titanium-Dioxide Nanotubes: Optical, Electronic and Magnetic Properties. *Nanoscale*, **6**, 10839-10849. https://doi.org/10.1039/c4nr02417f

[18] Behzad, S. and Chegel, R. (2013) Investigation of Magnetism in Aluminum-Doped Silicon Carbide Nanotubes. *Solid State Communications*, **174**, 38-42. https://doi.org/10.1016/j.ssc.2013.09.008

[19] Mabelet, L.B., Malonda-Boungou, B.R., Mabiala-Poaty, H.B., Raji, A.T. and M'Passi-Mabiala, B. (2020) Energetics, Electronic and Magnetic Properties of Monolayer WSe_2 Doped with Pnictogens, Halogens and Transition-Metal (4*d*, 5*d*) Atoms: An *ab-Initio* Study. *Physica E: Low-Dimensional Systems and Nanostructures*, **124**, Article ID: 114161. https://doi.org/10.1016/j.physe.2020.114161

[20] El-Khozondar, R.J. (2020) Monte Carlo Simulations of Topological Properties in Two-Phase Polycrystalline Materials for Several Diffusion Mechanism. *Advances in Pure Mathematics*, **10**, 471-491. https://doi.org/10.4236/apm.2020.109029

[21] Hwang, C. and Do, M. (2020) Fast Diffusion Monte Carlo Sampling via Conformal Map. *Applied Mathematics*, **11**, 35-41. https://doi.org/10.4236/am.2020.111004

[22] Hachem, N., Badrour, I.A., El Antari, A., Lafhal, A., Madani, M. and El Bouziani, M. (2021) Phase Diagrams of a Mixed-Spin Hexagonal Ising Nanotube with Core-Shell Structure. *Chinese Journal of Physics*, **71**, 12-21.

https://doi.org/10.1016/j.cjph.2020.07.001

[23] Kaneyoshi, T. (2011) Magnetic Properties of a Cylindrical Ising Nanowire (or Nanotube). *Physica Status Solidi* (*b*), **248**, 250-258. https://doi.org/10.1002/pssb.201046067

[24] Canko, O., Erdinç, A., Taşkın, F. and Fuat Yıldırım, A. (2012) Some Characteristic Behavior of Mixed Spin-1/2 and Spin-1 Ising Nano-Tube. *Journal of Magnetism and Magnetic Materials*, **324**, 508-513. https://doi.org/10.1016/j.jmmm.2011.08.046

[25] Wang, W., Liu, Y., Gao, Z., Zhao, X., Yang, Y. and Yang, S. (2018) Compensation Behaviors and Magnetic Properties in a Cylindrical Ferrimagnetic Nanotube with Core-Shell Structure: A Monte Carlo Study. *Physica E*: *Low-Dimensional Systems and Nanostructures*, **101**, 110-124. https://doi.org/10.1016/j.physe.2018.03.025

[26] Konstantinova, E. (2008) Theoretical Simulations of Magnetic Nanotubes Using Monte Carlo Method. *Journal of Magnetism and Magnetic Materials*, **320**, 2721-2729. https://doi.org/10.1016/j.jmmm.2008.06.007

[27] Karimou, M., Oke, T.D., Hontinfinde, S.I.V., Kple, J. and Hontinfinde, F. (2023) Mean-Field and Monte Carlo Calculations of Phase Transitions in a Core-Shell Ising Nanotube. *Physica B*: *Condensed Matter*, **666**, Article ID: 415107. https://doi.org/10.1016/j.physb.2023.415107

[28] Astaraki, M., Ghaemi, M. and Afzali, K. (2018) Investigation of Phase Diagrams for Cylindrical Ising Nanotube Using Cellular Automata. *Physics Letters A*, **382**, 1291-1297. https://doi.org/10.1016/j.physleta.2018.03.014

[29] Escrig, J., Landeros, P., Altbir, D., Vogel, E.E. and Vargas, P. (2007) Phase Diagrams of Magnetic Nanotubes. *Journal of Magnetism and Magnetic Materials*, **308**, 233-237. https://doi.org/10.1016/j.jmmm.2006.05.019

[30] Lv, B., Xu, Y., Wu, D. and Sun, Y. (2008) Preparation and Properties of Magnetic Iron Oxide Nanotubes. *Particuology*, **6**, 334-339. https://doi.org/10.1016/j.partic.2008.04.006

[31] Masrour, R., Bahmad, L., Hamedoun, M., Benyoussef, A. and Hlil, E.K. (2013) The Magnetic Properties of a Decorated Ising Nanotube Examined by the Use of the Monte Carlo Simulations. *Solid State Communications*, **162**, 53-56. https://doi.org/10.1016/j.ssc.2013.03.007

[32] Blume, M., Emery, V.J. and Griffiths, R.B. (1971) Ising Model for the λ transition and Phase Separation in He^3-He^4 Mixtures. *Physical Review A*, **4**, 1071-1077. https://doi.org/10.1103/physreva.4.1071

[33] Zounmenou, N.F., Hontinfinde, S.I.V., Kple, J., Karimou, M. and Hontinfinde, F. (2020) Magnetic Properties of a Spin-7/2 and Spin-5/2 Core/shell Nanowire: A Monte Carlo Study. *Applied Physics A*, **126**, Article No. 683. https://doi.org/10.1007/s00339-020-03856-0

[34] Metropolis, N., Rosenbluth, A.W., Rosenbluth, M.N., Teller, A.H. and Teller, E. (1953) Equation of State Calculations by Fast Computing Machines. *The Journal of Chemical Physics*, **21**, 1087-1092. https://doi.org/10.1063/1.1699114

[35] Karimou, M., Yessoufou, R.A., Ngantso, G.D., Hontinfinde, F. and Benyoussef, A. (2018) Mean-Field and Monte Carlo Studies of the Magnetic Properties of a Spin-7/2 and Spin-5/2 Ising Bilayer Film. *Journal of Superconductivity and Novel Magnetism*, **32**, 1769-1779. https://doi.org/10.1007/s10948-018-4876-4

[36] Diep, H.T. (2003) Physique de la Mattiere Condensée. Dunod.